Nanomechanical Characterisation of the Wood Cell Wall Using Atomic Force Microscopy

Olivier Arnould, Karl Bytebier, Pierre Cabrolier, Richard Arinero

NANOMECHANICAL CHARACTERISATION OF THE WOOD CELL WALL USING ATOMIC FORCE MICROSCOPY

O. Arnould, K. Bytebier
Laboratoire de Mécanique et Génie Civil, Université Montpellier 2/CNRS UMR5508
cc 048 – Place Eugène Bataillon, 34095 Montpellier
Téléphone : 04 67 14 96 50, Télécopie : 04 67 14 47 92
olivier.arnould@univ-montp2.fr

P. Cabrolier
Laboratoire des Ressources Forêt-Bois, AgroParisTech / INRA / UMR1092
14 rue Girardet, 54000, Nancy, France

R. Arinero
Institut d'Electronique du Sud, Université Montpellier 2/CNRS UMR5214
cc 082 – Place Eugène Bataillon, 34095 Montpellier
Téléphone : 04 67 14 32 98
richard.arinero@univ-montp2.fr

Keywords: wood, cell wall layers, (visco)elastic properties, Resonant Contact-AFM

1. INTRODUCTION

Wood is produced in successive cylindrical layers during the radial secondary growth of a tree by a very thin layer of living cells that divide, called cambium, and located under the bark. Wood is composed of different kinds of cells, with a honeycomb-like cellular organisation, and each plays a particular role for the tree. From a mechanical point of view, fibres are the cells that compose the structure (skeleton) of the tree (Thibaut *et al*, 2001). Figure 1 shows the idealized multi-layered structure of a typical wood fibre (typically around 1 mm long and around 20 μm in diameter). Each wood cell wall layer plays a particular role in the mechanical behaviour of wood and the elastic properties of wood originate mainly in those of its secondary cell wall layers. Each layer, particularly in the secondary wall, can be seen as a unidirectional long fibre composite whose fibres are cristalline (at around 70%) cellulosic microfibrils (as long as the cell and with some nm in diameter) and the matrix is made up of amorphous polymers: hemicelluloses, lignin and extractives (Salmén, 2004). The microfibrils are inclined to the cell axis by the so-called microfibril angle (MFA).

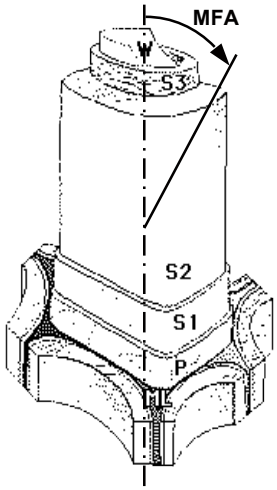

Figure 1. Idealized scheme of a typical fibre wall structure (adapted from Koch, 1985). The cell wall consists of: P-primary wall; S_1, S_2, S_3-layers of the secondary wall; W-warty layer; ML-middle lamella that binds cells together. Definition of the MicroFibrils Angle (MFA) for the S_2-layer. The empty part inside the fibre is called lumen.

Secondary walls are formed during cell differentiation by addition of constitutive material extruded from the plasma membrane and progressively incorporated into the wall. The mechanical properties of the wall depend on the amount of constitutive polymers, their spatial organisation, and also on the way they are bound to each other during cell development. To date, very little is known about how the mechanical properties of a wall layer progressively change during the early stages of its formation. Improved knowledge of the timing of wall stiffening may be useful to understand its assembly process. More specifically, it is necessary for understanding and modelling the apparition of maturation stress in wood (Archer, 1986; Thibaut *et al*, 2001; Yamamoto *et al*, 2002; Alméras *et al*, 2005; Coutand *et al*, 2007), because wall stiffness determines the

amount of stress generated by an impeded dimensional change of its constituents (Boyd, 1972). These maturation stresses allow the tree to improve its mechanical strength against bending loading (*e.g.,* wind or fruit weight) and to modify the shape of its trunk or branches by bending (Moulia *et al*, 2006). In this case, fibres act like a muscle for the tree and their (ultra)structure can be different from a classical one (*i.e.,* normal wood) in the case of strong reorientation where reaction wood is produced (Timell, 1986; Clair *et al*, 2006). Hardwood trees, for example, produce the so-called tension wood fibres that have a supplementary layer, generally in addition and inside the S_2-one, with a close to 0° MFA (Clair *et al*, 2006). This layer is usually called G-layer because its matrix is gelatinous (Clair *et al*, 2008).

Variability of wood cells distribution, thickness or properties lead to difficulties in the mechanical studies of wood at the macroscopic scale (*e.g.,* tree ring). Indeed, every tree has its own cellular organisation and structure that have a strong effect on the behaviour at upper (*i.e.,* macro) scales. Thus, nowadays, multi-scale modelling of wood is used to predict, for example, long-term behavior of wood in structural applications but it strongly needs measurements of its properties at the lowest level. Our goal is to measure mechanical properties within the different cell wall layers of mature fibres and, in a second time, their evolution during wall formation. Mechanical property measurements at the cell wall level can be estimated using numerical computations of the properties of its constituents or are more usually carried out experimentally on chemical compounds extracted from cell walls (Cousins, 1976; Cousins; 1978; Salmén, 2004) and on mechanically or chemically isolated fibres (Perez *et al*, 2000; Mott *et al*, 2002; Eder *et al*, 2008). Other measurements consisted in "classical" tensile tests on the scale of the tree rings or tissue using back-calculations (Cave and Hutt, 1969; Navi *et al*, 1995; Rüggeberg *et al*, 2008) and/or specific strain fields measurements (Fosberg *et al*, 2008; Réthoré *et al*, 2010). Technique based on FIB machining of the cell wall and micro-compression test has first been used recently (Zhang *et al*, 2010). In our case, it is necessary to have access to the *in situ* mechanical properties within cell walls with as few modifications as possible. Thus, one of the most promising and used techniques nowadays is nanoindentation. It has already been applied to estimate average elastic modulus of some wall layers of mature cells (Wimmer *et al*, 1997; Gindl *et al*, 2004; Tze *et al*, 2007; Konnerth *et al*, 2009) or to compare elastic properties of S_2 layers during the lignification process with those of mature cells (Gindl *et al*, 2002). However, this technique requires the layer thickness to be greater than the indent size (Gindl and Schöberlb, 2004), *i.e.,* typically greater than some micrometres. As the width of the cell wall layers varies from about 0.1 µm (primary wall) to less than 10 µm (mature S_2 and/or G layer), interpretation of measurements obtained by nanoindentation in the presence of a properties gradient or within a thin layer is not straightforward due to boundary effects (Jakes *et al*, 2009). Atomic Force Microscopy (AFM) allows one to do not only topography images at the nanometre scale but also to measure some (averaged) mechanical properties (elasticity, viscosity, etc) at this scale. Mechanical measurements done by Atomic Force Microscopy (AFM), using force-distance curves, force modulation microscopy, etc., require similar approaches as in nanoindentation but with a spatial resolution of the order of some tens of nanometre or less (Nysten, 2007). In our case, we used a specific mode of an AFM, sometimes called Resonant Contact-AFM (Arinero and Lévêque, 2003; Rabe, 2006; Nysten, 2007), that has already been applied on wood (Clair *et al*, 2003). It has been more recently improved with a mathematical processing that allows us to perform a quite fast mapping of mean viscoelastic properties (Arinero *et al*, 2007). The present article is restricted to the case of mature cells of chestnut tension wood and mainly focused on demonstrating the ability of this technique to obtain local semi-quantitative measurement and qualitative mapping of the viscoelastic properties at the ultrastructural level.

2. MATERIAL AND METHODS

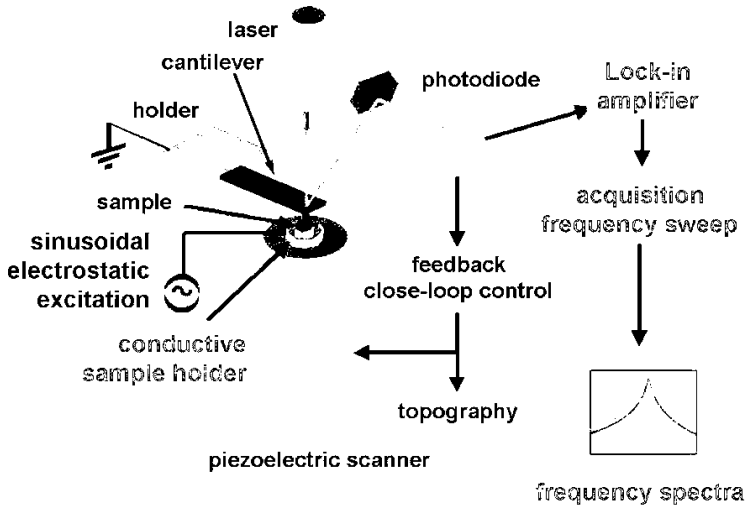

Figure 2. Schematic view of the basic principle of an AFM and its modification for doing Resonant Contact measurements with the use of a sinusoidal electrostatic excitation of the cantilever and a "lock-in" amplifier.

The basic principle of an AFM relies on measuring the interaction(s) of a physical probe, *i.e.,* a tip, with a sample surface (Figure 2). This interaction induces the bending of a very soft cantilever (*i.e.,* stiffness usually between 0.01 and 100 N/m) at the end of which the tip is. The angular deflection of this cantilever is measured through the reflection of a laser on its back

onto a position-sensitive photodetector. Relative in-plane (x, y) and out of plane (z) displacement of the sample *vs*. the probe is achieved through piezoelectric material actuators with a resolution better than 0.1 nm. There is a large variety of utilisation of AFM and way to measure the sample surface viscoelastic properties (Nysten, 2007). In the so-called contact mode, the tip remains in contact with the sample and the cantilever deflection is proportional to the applied contact force. As the tip scans the surface, a feedback loop keeps the contact force constant by adjusting the z-displacement of the actuator that is recorded and corresponds mainly to the surface topography. In that mode, since the tip touches the sample, it is sensitive to the sample viscoelastic properties. In this work, a specific operating contact mode, sometime called RC-AFM, was used (Arinero and Lévêque, 2003; Rabe, 2006; Nysten, 2007).

It consists in applying a small periodic force to the cantilever by means of an electrostatic potential between the tip and the sample holder (Figure 2). When the excitation frequency is close to the natural frequency of the cantilever, in contact with the sample surface through its tip, a resonance occurs. Basically, the measurement is based on performing a frequency sweep in a given point on the surface and recording the cantilever vibrations through the photodetector. According to several authors (Arinero and Lévêque, 2003; Rabe, 2006; Nysten, 2007), the resonance frequency, f_0, and the quality factor, Q, of the obtained frequency spectrum can be related respectively to the real, k', and imaginary, k", parts of the normal contact stiffness *at the resonance frequency*. It is then necessary to use the appropriated contact model to derive the elastic contact modulus M of the tested volume of material. The tangent of the loss angle, $\tan \delta = k"/k'$, which characterizes the viscous dissipation of the material in the tested volume is, in our case, close to Q^{-1} (if all other dissipations like tip sliding are negligible) for value of the quality factor higher than unity and is not dependant on the contact model (Arinero *et al*, 2007). The last step, as in all nanoindentation measurements, is to identify the material viscoelastic parameter(s). This is not so obvious in the case of an anisotropic and fibrous material such as the wood cell wall layers (Gindl and Schöberlb, 2004) even if anisotropic indentation model (Vlassak *et al*, 2003; Delafargue and Ulm, 2004) have been recently applied to a typical S_2 layer (Jäger *et al*, 2011) with reverse identification of some elastic properties (Konnerth *et al*, 2010). This aspect will not be presented in this paper. Finally, without any significant modification in the AFM device, this method theoretically offers submicrometre spatial resolution, as the mean and vibrating applied forces can be tuned as low as possible, and reduced lateral force effect due to the cantilever tilt angle. Moreover, by scanning the surface at a constant mean force and excitation frequency, close to the resonance of the different materials composing the area of interest, it is possible to do a reasonably fast mapping of the resonance frequency and quality factor whilst acquiring the sample topography without doing a frequency sweep at each point. This imaging technique is based on the cantilever vibration parameters (*i.e.,* the real and imaginary parts) that are directly linked to the parameters of the resonant spectrum of Lorentzian shape (Arinero *et al*, 2007).

In our case, a commercial AFM (Veeco Enviroscope) is used and its photodetector signal analysed by a lock-in amplifier (EG & G model 5302) to extract the real and the imaginary part of the cantilever vibration generated by the electrostatic excitation through an external generator (FLUKE PM5138A). In order to achieve the frequency sweep and resonance spectra acquisitions, an automated measurement was realized using Labview software and GPIB National Instruments interface. Our experiments show that the use of a theoretical model of cantilever vibration is not so obvious. This is why we decided here to use a series of "reference" materials like more or less stiff polymers (Polyurethane PU, Polyester PE, PMMA) and stiffer and less viscous materials like glass. The macroscopic viscoelastic properties of these materials have been measured at a frequency close to the one used during RC-AFM experiments (Cereser Camara *et al*, 2010). Frequency spectra are carried out on them and compared to the theoretical contact stiffness. The strongest assumption here is that these reference samples are assumed to be homogeneous even at the submicrometre scale and that properties at this scale are equal to those at the macroscopic level. In order to obtain as semi-quantitative as possible viscoelastic properties, it is moreover necessary to check the shape (*e.g.,* mean radius of curvature) of the AFM cantilever tip apex during calibration and experiments on wood. The main problem arising during the experiment is that, as the tip is always in contact with the surface during imaging, more or less wear occurs and can lead to a drastic change in the tip apex shape. It is then necessary to have a fast way to characterise the shape between two measurements. We compared different calibration gratings and SEM images and have finally chosen a calibration grating (NT-MDT TGT-01) that consists in an array of very sharp spikes with a radius lower than about 8 nm. It allows for some kind of (fast) reverse imaging of the actual apex shape with enough accuracy in the present case. The (average) technical specifications of the cantilever used for the experiments (Nanoworld Arrow FMR) are: thickness 3 µm, length 240 µm, width 35 µm, stiffness 2.8 N/m, free natural frequency 75 kHz. The average tip radius is estimated to be around 55 nm during the measurements. The mean applied force is estimated to be around 180 nN and the sinusoidal electrostatic excitation is applied with an amplitude of 10 V.

In order to investigate the RC-AFM imaging technique in the case of wood, chestnut (*Castanea sativa*) mature wood containing normal as well as tension wood was used. Tension wood is characterized, in the case of chestnut, by the presence of a G layer and a thin S_2-layer. All mechanical measurement based on indentation requires samples with a surface as flat as possible compared to the contact radius in order to be able to estimate accurately the contact area. Moreover, in the case of AFM, the tip is very brittle and surface roughness (or holes) must be as low as possible to reduce breakage risks. Wood samples were then embedded in a resin in order to fill the lumen and to decrease the surface roughness by reducing deformation during the cutting process. Sticks (1 cm in longitudinal direction, 1 × 1 mm² in transverse section) were obtained by splitting to guarantee a good axial direction. They were then cut manually with a razor blade to produce a clear transverse surface and to obtain cubes of about 1 mm^3 in size. Samples were dehydrated with an ethanol series (50%, 75%, 90% and 100%) under vacuum and embedded in increasing ratio of LR White medium resin. The whole resin block with the sample

was then machined to reduce its cross section. A rotary microtome (Leica RM2235) was then used first with a glass knife to remove the first 100 µm of material containing the border effects that occurs during initial sample preparation (Clair *et al*, 2005). Then a diamond knife (Diatom Histo) was used to cut a series of very thin section (about 500 nm in thickness) at the lowest cutting speed to minimize compression during the cutting process. The resulting topography of the remaining wood block sample surface is obtained during the mechanical measurement in RC-AFM mode and shown in Figure 3. Some steps in the topography due to difference in the stiffness of the different layers are observed. However, the typical Root-Mean-Square (RMS) roughness in the thicker, G and S_2, layers is usually around 10 nm.

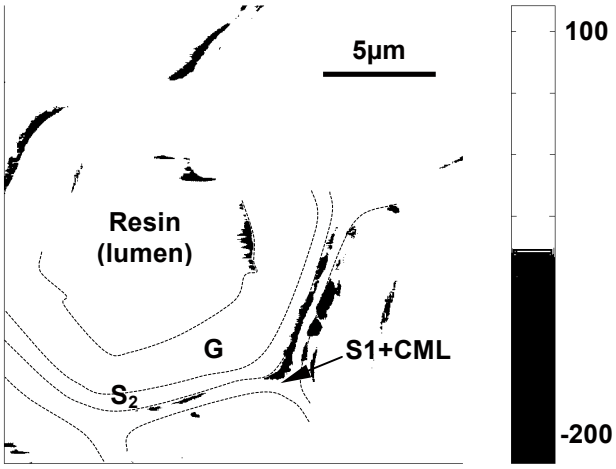

Figure 3. AFM topography (256 × 256 points) in contact mode of the chestnut tension wood cross section. Identification of the different cell wall layers and of the embedding LR White resin in the cell lumina. CML stands for compound middle lamella and corresponds to the middle lamella and the primary wall (Figure 1).
The scale bar corresponds to the height in nm.

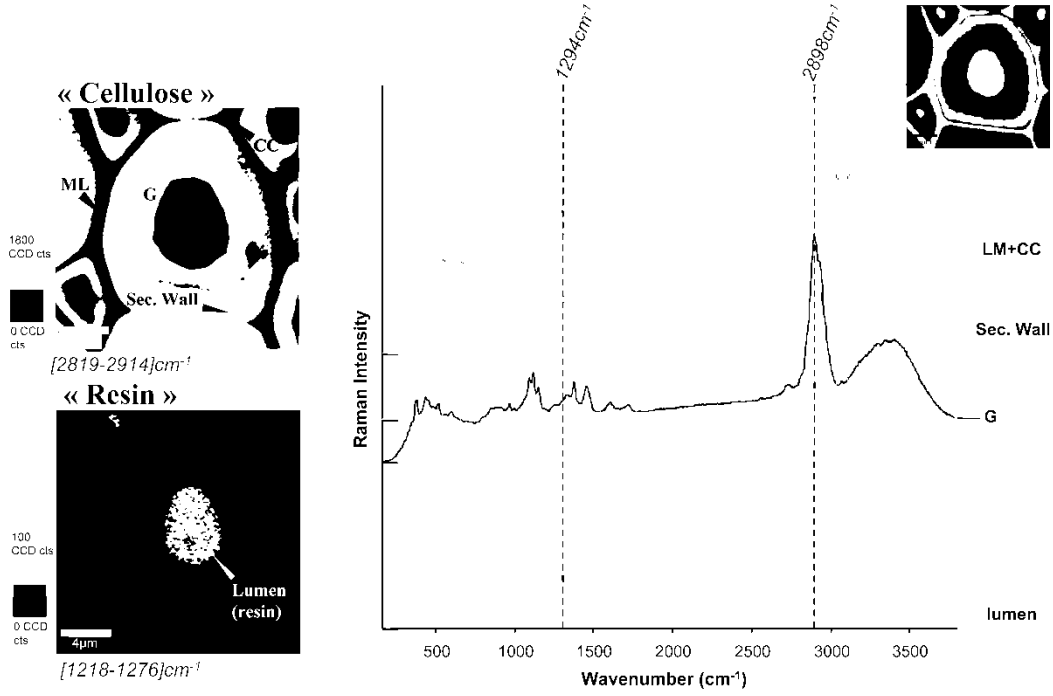

(a) (b)

Figure 4. a) Raman mappings of chestnut tension wood cells by integrating 2 characteristics Raman bands on all pixels. Top image correspond to "cellulose" and reveal gelatinous layer (G), secondary cell wall (Sec. Wall), and by contrast middle lamella (ML) and cell corner (CC). Bottom mapping highlights only the lumen, and in this case resin. b) Average spectrum superposed of selected zones (CC and ML, G, Sec. Wall and Lumen, image on top right). Red ellipses indicate the resin contribution in the cell walls spectrums.

Finally, a confocal Raman microspectrometer system (WiTec Alpha 300 R) have been used in order to describe chemical distribution at the sub-cell wall level, and more particularly to evaluate resin penetration in the cell wall. Raman microscopy is a nondestructive in situ tool for chemical mapping with a high resolution (Agarwal, 2006; Gierlinger and Schwanninger, 2006). An oil objective, with a numerical aperture of 1.4 (Nikon 60X), combined with a green laser excitation (532 nm

wavelength) provide the best results in term of lateral resolution, approximately 230 nm. Thin cross section (3 µm) have been cut with a diamond knife mounted on a rotary ultramicrotome (Leica EM UC6), and placed between a glass slide with a drop of water and a coverslip surrounded by viscous grease to prevent evaporation due to laser heat. Raman scan has been realized by overlapping (pixel size of 0.13 µm). The diffraction spot size of 100 µm has been chosen to keep maximum Raman light to the detriment of the depth resolution in order to decrease the integration time per pixel at 0.06 s. For all pixels corresponds a single spectrum that has been analyzed with the software WiTec Control. Raman Spectrometer (UHTS 300) provides a spectral resolution of 4 cm^{-1}. By integrating with a sum filter over identified wavenumber areas in the spectrum, chemicals imaging have been realized. Raman band from 2819 to 2914 cm^{-1} (Figure 4a top) knows as CH and CH2 stretching vibration correspond to carbohydrates, and more particularly cellulose. Higher intensity highlights the gelatinous layer (G), the secondary cell wall (Sec. Wall) and by contrast, darker regions reveals middle lamella (ML) and cell corner (CC). The band between 1218 and 1276 cm^{-1} unidentified here, highlights lumens and in this case resin of the impregnated sample (Figure 4a bottom). It appears that resin is only concentrated in the lumen. After a selection of zones, by marking distinct regions (CC and ML, G, Sec. Wall and lumen) average spectrum have been calculated using the software Witec Project (Figure 3b). Comparing with cell walls average spectrums of a chestnut sample not impregnated (results not presented in this paper), it appears that resin spectrum have a small contribution in the cell walls spectrums (red ellipses in Figure 4b). With regard to the small contribution in term of resin band intensity in the cell walls average spectrums, it seems possible to assume a weak penetration of the resin in the cell wall.

3. RESULTS AND DISCUSSION

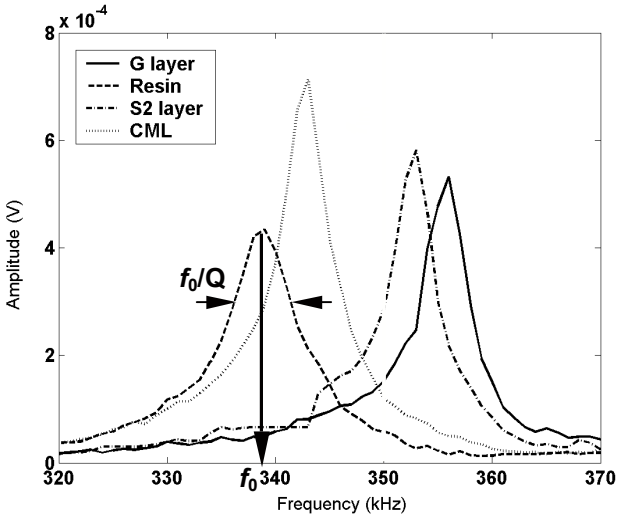

Figure 5. Amplitude frequency spectrum for the different layers. Definition of the resonance frequency f_0 and quality factor Q in the case of the embedding resin. Choice of the imaging frequency f_{im} for Figure 6.

The RC-AFM experiments are done in two steps. The first step is to engage the tip in contact with the sample and to carry out frequency spectra at different points. In Figure 5, the amplitude of the output signal of the photodetector is plotted as a function of the electrostatic excitation frequency. The resonance frequency f_0 and the quality factor Q of the frequency spectrum in each layer are then deduced. The indentation modulus in the longitudinal direction M_L is then computed using the different calibrations done (as depicted in the previous chapter). The results are given in Table 1. They correspond to the mean values obtained from at least 3 spectra done in 3 different positions within the same layer. The uncertainty in this table only represents the variation in the value computed from one point to another. It doesn't take into account all the uncertainty coming from the different calibration steps and measurements accuracy that can be much higher and must be estimated. These results are consistent with those obtain previously on oak (Clair *et al*, 2003) and other S_2 cell wall layer (Wimmer et al, 1997; Gindl *et al*, 2004; Tze *et al*, 2007; Konnerth *et al*, 2009). Moreover, using an elastic anisotropic indentation model (Delafargue and Ulm, 2004) and a multi-scale cell wall model (Alméras *et al*, 2005) with the estimated elastic properties of the cell wall constituents given in (Salmén, 2004) and a given composition of the S_2 or G layer (*i.e.,* 30% crystalline cellulose and 70% amorphous cellulose and matrix material), leads to an indentation modulus around 16 GPa for an MFA of 0°. The results obtained by RC-AFM seem quite good in average given all the assumption made on the composition of the layer, the properties of its constituent and the fact that the MFA of the S_2 layer is not known. The fact that they are lower may be explained by the fibrous nature of the material that could lead to different contact behaviour even when anisotropy is taken into account. Moreover, this fibrous structure leads to nanometre topography during the cutting process (Falhén and Salmén, 2005). This nano-roughness can lead to an underestimation of the real contact area using a classical contact model that assumes a perfectly flat surface, and yields an estimated indentation modulus lower than the real one. Moreover, the indentation model used is developed for pyramidal (deep) indentation and not for a sphere-plane contact. Finally, measurements in progress show that the accuracy and sensitivity of the RC-AFM to the elastic modulus can be improved by using a stiffer cantilever.

Table 1. Indentation modulus ML and reverse of the quality factor Q^{-1}(~ tan δ at the resonance frequency) in the longitudinal direction for the different layers of the cell wall computed from the spectra of Figure 5. Specified uncertainties only correspond to the variations between 3 measurement locations.

	M_L (GPa)	Q^{-1}
Resin	6±1.5	0.013±0.002
CML	6.5±0.5	0.009±0.003
S_2	12±0.5	0.006±0.003
G	14±1.5	0.009±0.003

The last step of the measurement is to do a mapping at a given excitation frequency f_{im}. To be able to compute the resonance frequency and quality factor from the real and imaginary parts of the cantilever vibration, f_{im} must be chosen as close as possible to the resonance frequency on each layer. In the present case, as we want to demonstrate the ability of this technique to sense differences in mechanical properties mainly in the S_2 and G layers, the imaging frequency is chosen close to that obtained on these layers (Figure 5). As a result, the mechanical properties of the embedding resin and, to a less extent, that of the CML will be poorly estimated. The resulting indentation modulus and reverse of the quality factor maps are given in Figure 6 for an imaging frequency of 350 kHz. In Figure 6a, the S_2 and G layers clearly appear to be the stiffest ones in average whereas the S_1 and CML layers are the softest as in Table 1. Layers appear far more clearly than in the topography image of Figure 3. Variations in the indentation modulus of the S_2 layer are observed. These variations could be due to natural gradient properties within the layer (*e.g.,* tangential *vs*. radial wall) or to local variation in the MFA (Sedighi-Gilani *et al*, 2006). But it appears that theyr are mainly due to a slightly oblique cross section combined with the MFA that induce a different type of loading with respect to the microfibrils axis (Konnerth *et al*, 2009): the highest frequencies would then mean a loading closer to the microfibril axis than the lowest values. In the latter case, contribution of the matrix in the measured frequency is higher. Furthermore, G layers sometime appear to be composed of two slightly different stiffness parts (see the two arrows in Figure 6). We don't know if it's a real property variation in the layer or if it's due to the embedding protocol as resin penetration within the cell wall may change the measured viscoelastic properties. However, it can be inferred that resin presence in the gel of the G layer should increase the elastic modulus. Lastly, it can be seen that topography (*e.g.,* scratches due to the cutting and step height to a less extent, see Figure 3) has an effect on the measurement such as roughness. Whatever the real origin of all these observations, it demonstrates the ability of the RC-AFM to highlight elastic properties variations within a single cell wall layer.

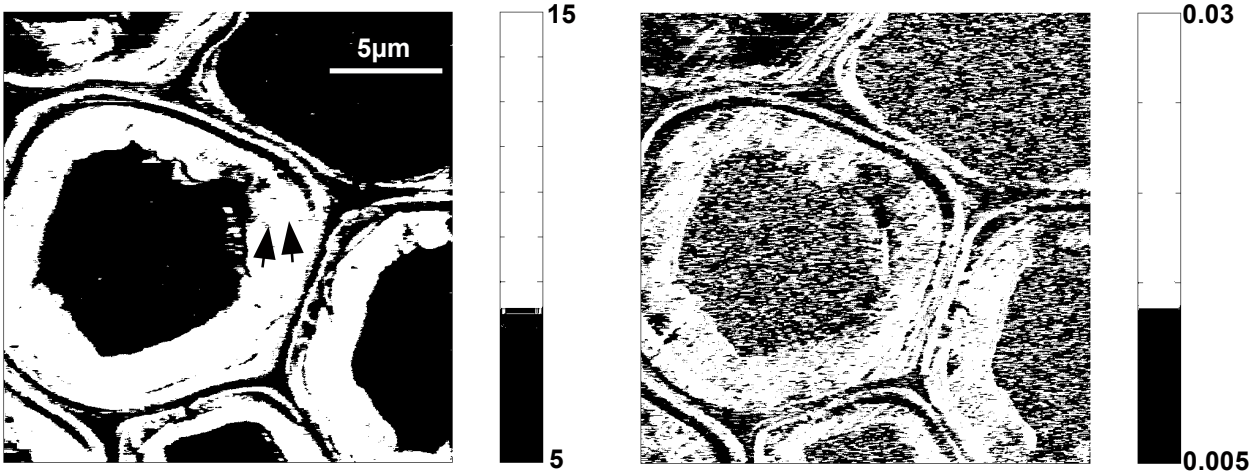

(a) (b)

Figure 6. Semi-quantitative mapping at 350 kHz in the same area as in Figure 3: a) longitudinal indentation modulus M_L – scale bar in GPa; b) reverse of the quality factor Q^{-1} (~ tan δ at the resonance frequency).

For the viscous parameter, tan δ in Figure 6b, results are not so clear as the CML seems to be surprisingly less viscous than the S_2 layer whereas the S_1 is more. This contradicts the values of Q^{-1} obtained in Table 1 and it seems to be mostly due to the choice in the imaging frequency that is too far from the resonance of the CML (*e.g.,* see the noise in the resin part). It is interesting to note that, on average, the G layer is more viscous than the S_2 as in Table 1. The assumption we made above on the origin of the elastic variations in the S_2 layer due to a slightly oblique cross section is not really confirmed here. If the indentation modulus increased because the microfibril axis is closer to the contact normal, the mechanical contribution of the matrix is lower and then the dissipation too. Again, the effect of the fibrous nature of the layers, and the resulting cutting nano-roughness, on the contact properties are questioned. Note that topography has a stronger effect in that case. Lastly, one can wonder what is the physical meaning (in the frame of tree biomechanics or usual use of wood as a material) of a viscous parameter obtained at a so high frequency. More work has to be done on this aspect of the measurements.

4. CONCLUSION

This study shows that RC-AFM allows for semi-quantitative estimation of stiffness in a given point and qualitative estimation of its variations at a submicrometre scale. Studies are in progress on improving its calibration and the experimental conditions to make it more quantitative for the estimation of viscoelastic properties. This technique should be able to provide data on the stiffness gradient within the cell wall and its evolution during the maturation process. Moroever, closer views of the G layer topography, indentation modulus and dissipation were made and structures with typical size around 50 to 100 nm were highlight. They could be ascribed to microfibrils bundles, whose size is typically around 20 nm in softwoods (Fahlén and Salmén, 2005) and hardwoods (Ruelle *et al*, 2007), with a classical tip dilation effect. This shows again the ability of AFM to study the mechanical properties of the cell wall at the ultrastructural scale. However, concerning the estimates of viscous properties of the material, some questions remain on their significance during these kinds of measurements especially at the lowest scale. An other AFM technique, called UFM (Cuberes *et al*, 2007), has been recently used on a similar sample and gives first encouraging results at the microfibrils scale. In the case of developing cells, the sample preparation is not so obvious as for mature cells. Resin penetration can be stronger in that case and have a higher effect on the measurement as the cell wall is softer. First tests on samples of developing cells taken along a differentiation sequence, from the cambium to the mature wood, are currently done using the above embedding technique and an other kind of embbeding resin, known to not penetrate the cell wall of mature cell (Konnerth *et al*, 2009), will be tried soon.

ACKNOWLEDGEMENTS

Financial support by the CNRS, the University of Montpellier 2 and the COST action FP0802 is gratefully acknowledged.

REFERENCES

Agarwal U.P., “Raman imaging to investigate ultrastructure and composition of plant cell walls: distribution of lignin and cellulose in black spruce wood (*Picea mariana*)”, *Planta*, **224**, (2006), pp. 1141-1153.

Alméras T., Gril J. and Yamamoto H., “Modeling anisotropic maturation strains in wood in relation to fibre boundary conditions, microstructure and maturation kinetics”, *Holzforschung*, **59**, (2005), pp. 347-353.

Archer R.R., “Growth stresses and strains in trees”, In: *Springer Series in Wood Science*, Timell E. (Ed.), Springer-Verlag, Berlin, (1986), p. 240.

Arinero R. and Lévêque G., “Vibration of the cantilever in Force Modulation Microscopy analysis by a finite element model”, *Review of Scientific Instruments*, **74**, (2003), pp. 104-111.

Arinero R., Lévêque G., Girard P. and Ferrandis J.Y., “Image processing for resonance frequency mapping in atomic force microscopy”, *Review of Scientific Instruments*, **78**, (2007), 6p.

Boyd J.D., “Tree growth stresses. Evidence of an origin in differenciation and lignification”, *Wood Science and Technology*, **6**, (1972), pp. 251-262.

Cave I.D. and Hutt L., “The Longitudinal Young's Modulus of *Pinus Radiata*”, *Wood Science and Technology*, **3**, (1969), pp. 40-48.

Cereser Camara V., Laux D. and Arnould O., “Enhanced multiple ultrasonic shear reflection method for the determination of high frequency viscoelastic properties”, *Ultrasonics*, **50**, (2010), pp. 710-715.

Clair B., Arinero R., Lévêque G., Ramonda M. and Thibaut B., “Imaging the mechanical properties of wood cell wall layers by atomic force modulation microscopy”. *IAWA Journal*, **24**, (2003), pp. 223-230.

Clair B., Gril J., Baba K., Thibaut B. and Sugiyama J., “Precautions for the structural analysis of the gelatinous layer in tension wood”, *IAWA Journal*, **26**, 2, (2005), pp. 189-195.

Clair B., Ruelle J., Beauchêne J., Prévost M.F. and Fournier M., “Tension wood and opposite wood in 21 tropical rain forest species. 1. Occurrence and efficiency of G-layer”, *IAWA Journal*, **27**, 3, (2006), pp. 329-338.

Clair B., Gril J., Di Renzo F., Yamamoto H. and Quignard F., “Characterization of a gel in the cell wall to elucidate the paradoxical shrinkage of tension wood”, *Biomacromolecules*, **9**, (2008), pp. 494-498.

Cousins W.J., “Elastic Modulus of Lignin as Related to Moisture Content”, Wood Science and Technology, **10**, (1976), pp. 9-17.

Cousins W.J., “Young's modulus of hemicellulose as related to moisture content”, *Wood Science and Technology*, **12**, (1978), pp. 161-167.

Coutand C., Fournier M. and Moulia B., “The gravitropic response of poplar trunks: Key roles of prestressed wood Regulation and the relative kinetics of cambial growth versus wood maturation”, *Plant Physiology*, **144**, (2007), pp. 1166-1180.

Cuberes M.T., Stegemann B., Kaiser B. and Rademann K., “Ultrasonic force microscopy on strained antimony nanoparticles”, *Ultramicroscopy*, **107**, (2007), pp. 1053–1060.

Delafargue A. and Ulm F.J., “Explicit approximations of the indentation modulus of elastically orthotropic solids for conical indenters”, *International Journal of Solids and Structures*, **41**, (2004), pp. 7351-7360.

Eder M., Stanzl-Tschegg S. and Burgert I., “The fracture behaviour of single wood fibres is governed by geometrical constraints: in situ ESEM studies on three fibre types”, *Wood Science and Technology*, **42**, (2008), pp. 679-689.

Falhén J. and Salmén L., "Ultrastructural changes in a holocellulose pulp revealed by enzymes, thermoporosimetry and atomic force microscopy", *Holzforschung*, **59**, (2005), pp. 589-597.

Forsberg F., Mooser R., Arnold M., Hack E. and Wyss P., "3D micro-scale deformations of wood in bending: Synchrotron radiation μCT data analyzed with digital volume correlation", *Journal of Structural Biology*, **164**, 3, (2008), pp. 255-262.

Gierlinger N. and Schwanninger M., "Chemical imaging of poplar wood cell walls by confocal Raman microscopy", *Plant Physiology*, **140**, (2006), pp. 1246-1254.

Gindl W., Gupta H.S. and Grünwald C., "Lignification of spruce tracheid secondary cell walls related to longitudinal hardness and modulus of elasticity using nano-indentation", *Canadian Journal of Botany*, **80**, (2002), pp. 1029-1033.

Gindl W., Gupta H.S., Schöberl T., Lichtenegger H.C. and Fratzl P. "Mechanical properties of spruce wood cell walls by nanoindentation", *Applied Physics A: Materials Science & Processing*, **79**, 8, (2004), pp. 2069-2073.

Gindl W. and Schöberlb T., "The significance of the elastic modulus of wood cell walls obtained from nanoindentation measurements", *Composites: Part A*, **35**, (2004), pp. 1345–1349.

Jäger A., Bader Th., Hofstetter K. and Eberhardsteiner J., "The relation between indentation modulus, microfibril angle, and elastic properties of wood cell wall", *Composites: Part A*, (2011), doi: 10/1016/j.compositesa.2011.02.07.

Jakes J.E., Frihart C.R., Beecher J.F., Moon R.J., Resto P.J., Melgarejo Z.H., Suarez O.M., Baumgart H., Elmustafa A.A and Stone D.S., "Nanoindentation near the edges", *Journal of Materials Research*, **24**, 3, (2009), pp. 1016-1031.

Konnerth J., Gierlinger N., Keckes J. and Gindl W., "Actual versus apparent within cell wall variability of nanoindentation results from wood cell walls related to cellulose microfibril angle", *Journal of Materials Science*, **44**, (2009), pp. 4399-4406.

Konnerth J., Buksnowitz C., Gindl W., Hofstetter K. and Jäger A., "Full set of elastic constants of spruce wood cell walls determined by nanoindentation", In: *Proceedings of the International Convention of Society of Wood Science and Technology and United Nations Economic Commission for Europe – Timber Committee*, Geneva, Switzerland, October 11-14, (2010), 9p.

Mott L., Groom L. and Shaler S., "Mechanical properties of individual southern pine fibers, Part I: comparison of early wood and late wood fibers with respect to tree height and juvenility", *Wood and Fiber Science*, **34**, 2, (2002), pp. 221-237.

Moulia B., Coutand C. and Lenne C., "Posture control and skeletal mechanical acclimation in terrestrial plants: implications for mechanical modeling of plant architecture", *American Journal of Botany*, **93**, (2006), pp. 1477-1489.

Navi P., Rastogi P.K., Gresse V. and Tolou A., "Micromechanics of wood subjected to axial tension", Wood Science and Technology, **29**, 6, (1995), pp. 411-429.

Nysten B., *Nanomechanics with the Atomic Force Microscope: Polymer surfaces, interfaces and nanomaterials*, Associate Professor Thesis, Université Catholique de Louvain, Belgium, (2007), 228 p.

Perez L., Pittet V. and Navi P., "Fiber behaviour under tensile force, experimentation and modelling", In: *Proceedings of the International Conference on Wood and Wood Fibre Composites*, Aicher S. (Ed), Stuttgart, Germany, (2000), pp. 47-58.

Rabe U., "Atomic force acoustic microscopy" In: *Applied Scanning Probe Methods II: Scanning Probe Microscopy Techniques*, Bhushan B. and Fuchs H. (Eds), Springer-Verlag, Berlin, (2006), pp. 36-90.

Réthoré J., Simon P. and Maigre H., "Multiscale digital image identification of heterogeneous elastic properties of softwoods", *EPJ Web of Conferences*, **6**, 18002, (2010), 7p.

Rüggeberg M., Speck T., Paris O., Lapierre C., Pollet B., Koch G. and Burgert I., "Stiffness gradients in vascular bundles of the palm *Washingtonia robusta*", Proceedings of the Royal Society B, **275**, (2008), pp. 2221-2229.

Ruelle J., Yoshida M., Clair B. and Thibaut B., "Peculiar tension wood structure in Laetia procera (Poepp.) Eichl. (Flacourtiaceae)", *Trees*, **21**, (2007), pp. 345-355.

Salmén L., "Micromechanical understanding of the cell-wall structure", *Comptes Rendus Biologies*, **327**, (2004), pp. 873-880.

Salmén L. and Burgert I., "Cell wall features with regard to mechanical performance. A Review", *Holzforschung*, **62**, (2008), pp. 121-129.

Sedighi-Gilani M., Sunderland H. and Navi P., "Within-fiber non-uniformities of microfibril angle", *Wood and Fiber Science*, 38, 1, (2006), pp. 132-138.

Thibaut B., Gril J. and Fournier M., "Mechanics of wood and trees: some new highlights for an old story", *Comptes Rendus de l'Académie des Sciences Paris*, *Série II b*, **329**, (2001), pp. 701-716.

Timell T. E., *Compression wood in gymnosperms*, Vol. 1, Springer Verlag, (1986).

Tze W.T.Y., Wang S., Rials T.G., Pharr G.M. and Kelley S.S., "Nanoindentation of wood cell walls: Continuous stiffness and hardness measurements", *Composites: Part A*, **38**, (2007), pp. 945-953.

Vlassak J.J., Ciavarella M., Barber J.R. and Wang X., "The indentation modulus of elastically anisotropic materials for indenters of arbitrary shape", *Journal of the Mechanics and Physics of Solids*, **51**, (2003), 1701-1721.

Wimmer R., Lucas B.N., Tsui T.Y and Oliver W.C., "Longitudinal hardness and Young's modulus of spruce tracheid secondary walls using nanoindentation technique", *Wood Science and Technology*, **31**, (1997), pp. 131-141.

Yamamoto H., Kojima Y., Okuyama T., Abasolo W.P. and Gril J., "Origin of the biomechanical properties of wood related to the fine structure of the multi-layered cell wall", *Transactions of the ASME*, 124, (2002), pp. 432-440.

Zhang X., Zhao Q., Wanga S., Trejo R., Lara-Curzio E. and Dud G., "Characterizing strength and fracture of wood cell wall through uniaxial micro-compression test", *Composites: Part A*, **41**, (2010) , pp. 632-638.